

O₂ and CO Binding Properties of Artificial Hemoproteins Formed by Complexing Iron Protoporphyrin IX with Human Serum Albumin Mutants

Teruyuki Komatsu,^{*,†} Naomi Ohmichi,[†] Akito Nakagawa,[†] Patricia A. Zunszain,[‡] Stephen Curry,[‡] and Eishun Tsuchida^{*,†}

Contribution from the Advanced Research Institute for Science and Engineering, Waseda University, 3-4-1 Okubo, Shinjuku-ku, Tokyo 169-8555, Japan, and Division of Cell and Molecular Biology, Faculty of Life Sciences, Imperial College London, Huxley Building, South Kensington Campus, London SW7 2AZ, United Kingdom

Received July 18, 2005; E-mail: teruyuki@waseda.jp; eishun@waseda.jp

Abstract: The binding properties of O₂ and CO to recombinant human serum albumin (rHSA) mutants with a prosthetic heme group have been physicochemically and kinetically characterized. Iron(III) protoporphyrin IX (hemin) is bound in subdomain IB of wild-type rHSA [rHSA(wt)] with weak axial coordination by Tyr-161. The reduced ferrous rHSA(wt)-heme under an Ar atmosphere exists in an unusual mixture of four- and five-coordinate complexes and is immediately autoxidized by O₂. To confer O₂ binding capability on this naturally occurring hemoprotein, a proximal histidine was introduced into position Ile-142 or Leu-185 by site-directed mutagenesis. A single mutant (I142H) and three double mutants (I142H/Y161L, I142H/Y161F, and Y161L/L185H) were prepared. Both rHSA(I142H/Y161L)-heme and rHSA(I142H/Y161F)-heme formed ferrous five-N-coordinate high-spin complexes with axial ligation of His-142 under an Ar atmosphere. These artificial hemoproteins bind O₂ at room temperature. Mutation at the other side of the porphyrin, Y161L/L185H, also allowed O₂ binding to the heme. In contrast, the single mutant rHSA(I142H)-heme could not bind O₂, suggesting that removal of Y161 is necessary to confer reversible O₂ binding. Laser flash photolysis experiments showed that the kinetics of CO recombination with the rHSA(mutant)-heme were biphasic, whereas O₂ rebinding exhibited monophasic kinetics. This could be due to the two different geometries of the axial imidazole coordination arising from the two orientations of the porphyrin plane in the heme pocket. The O₂ binding affinities of the rHSA(mutant)-heme were significantly lower than those of hemoglobin and myoglobin, principally due to the high O₂ dissociation rates. Changing Leu-161 to Phe-161 at the distal side increased the association rates of both O₂ and CO, which resulted in enhanced binding affinity.

Introduction

Human serum albumin (HSA) is a versatile protein found at high concentrations (4–5 g/dL) in blood plasma and is principally characterized by its remarkable ability to bind a wide range of insoluble endogenous and exogenous compounds.¹ Physiological ligands for HSA include nonesterified fatty acids, hemin, bilirubin, bile acids, and thyroxine,^{2–4} but the protein

also binds a huge variety of drugs. Currently, it is of great interest to exploit the carrier properties of this shuttle protein for the development of novel therapeutic reagents for drug delivery and pharmacodynamic modulation.^{5–7} Hemin [iron(III) protoporphyrin IX] released from hemoglobin (Hb) during the enucleation of red cells or through hemolysis is captured by HSA, which has a high binding constant for this ligand ($K \approx 10^8 \text{ M}^{-1}$).⁸ This strong affinity of HSA for hemin has stimulated efforts to develop albumin as an artificial hemoprotein which can mimic the O₂ binding capability of Hb and myoglobin (Mb).^{9,10} HSA consists of a helical monomer of 66.5 kDa containing three homologous domains (I–III), each of which

[†] Waseda University.

[‡] Imperial College London.

- (1) Peters, T. *All about Albumin: Biochemistry, Genetics and Medical Applications*; Academic Press: San Diego, 1996; and references therein.
- (2) (a) Kragh-Hansen, U. *Pharmacol. Rev.* **1981**, *33*, 17–53. (b) Kragh-Hansen, U. *Danish Med. Bull.* **1990**, *37*, 57–84.
- (3) (a) Curry, S.; Madelkow, H.; Brick, P.; Franks, N. *Nat. Struct. Biol.* **1998**, *5*, 827–835. (b) Bhattacharya, A. A.; Grune, T.; Curry, S. *J. Mol. Biol.* **2000**, *303*, 721–732. (c) Curry, S. Plasma Albumin as a Fatty Acid Carrier. In *Adv. Mol. Cell. Biol.*; van der Vusse, G., Ed.; Elsevier: 2003; Vol. 33, pp 29–46. (d) Petipas, I.; Petersen, C. E.; Ha, C.-E.; Bhattacharya, A. A.; Zunszain, P. A.; Ghuman, J.; Bhagavan, N. V.; Curry, S. *Proc. Natl. Acad. Sci. U.S.A.* **2003**, *100*, 6440–6445. (e) Zunszain, P. A.; Ghuman, J.; Komatsu, T.; Tsuchida, E.; Curry, S. *BMC Struct. Biol.* **2003**, *3*, 6.
- (4) (a) He, X. M.; Carter, D. C. *Nature* **1992**, *358*, 209–215. (b) Carter, D. C.; Ho, J. X. *Adv. Protein Chem.* **1994**, *45*, 153–203. (c) Wardell, M.; Wang, Z.; Ho, J. X.; Robert, J.; Ruker, F.; Rubel, J.; Carter, D. C. *Biochem. Biophys. Res. Commun.* **2002**, *291*, 813–819.

- (5) Beljaars, L.; Molema, G.; Schuppan, D.; Geerts, A.; De Bleser, P. J.; Weert, B.; Meijer, D. K. F.; Poelstra, K. *J. Biol. Chem.* **2000**, *275*, 12743–12751.
- (6) Kurtzhals, P.; Havelund, S.; Jonassen, I.; Kiehr, B.; Larsen, U. D.; Ribel, U.; Markussen, J. *Biochem. J.* **1995**, *312*, 725–731.
- (7) Sheffield, W. P. *Curr. Drug Targets Cardiovasc. Haematol. Disord.* **2001**, *1*, 1–22.
- (8) Adams, P. A.; Berman, M. C. *Biochem. J.* **1980**, *191*, 95–102.
- (9) (a) Komatsu, T.; Hamamatsu, K.; Wu, J.; Tsuchida, E. *Bioconjugate Chem.* **1999**, *10*, 82–86. (b) Tsuchida, E.; Komatsu, T.; Matsukawa, Y.; Hamamatsu, K.; Wu, J. *Bioconjugate Chem.* **1999**, *10*, 797–802. (c) Komatsu, T.; Matsukawa, Y.; Tsuchida, E. *Bioconjugate Chem.* **2002**, *13*, 397–402.

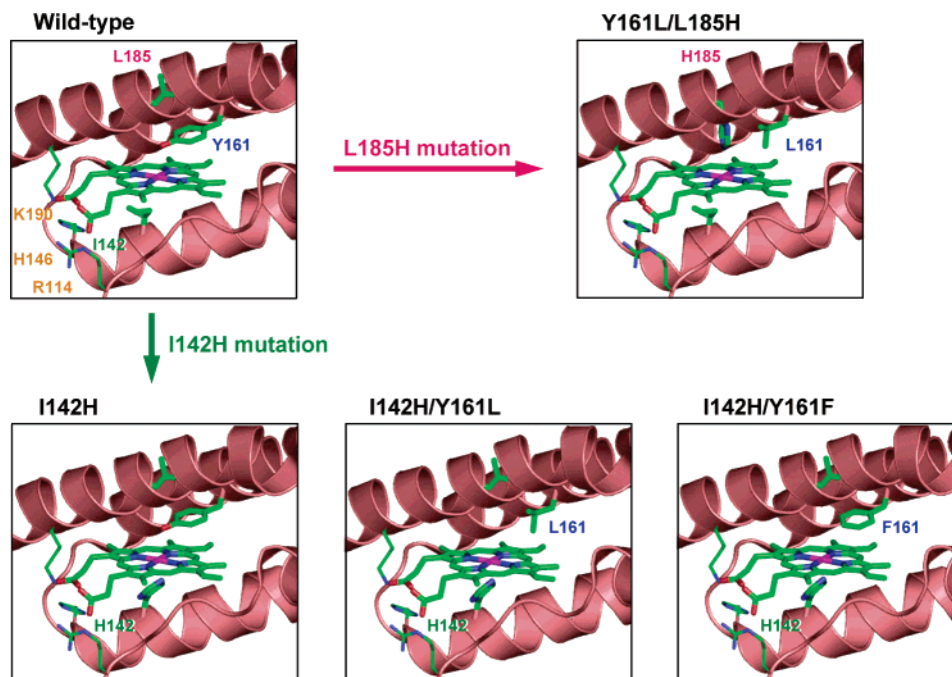


Figure 1. Structural models of the effect of site-directed mutagenesis in subdomain IB of HSA to construct a tailor-made heme pocket, which allows O₂ binding to the prosthetic Fe²⁺ protoporphyrin IX (heme) group.¹²

is composed of A and B subdomains. Crystallographic studies have revealed that heme is bound within a narrow D-shaped hydrophobic cavity in subdomain IB with axial coordination of Tyr-161 to the central ferric ion and electrostatic interactions between the porphyrin propionates and a triad of basic amino acid residues (Arg-114, His-146, and Lys-190) (Figure 1).^{3e,4c} In terms of the general hydrophobicity of this α -helical heme pocket, the subdomain IB of HSA potentially has similar features to the heme binding site of Hb or Mb. However, if one reduces the HSA–hemin to obtain the ferrous complex, it is rapidly oxidized by O₂ even at low temperature (~ 0 °C). This is due to the fact that HSA lacks the proximal histidine which in Hb and Mb enables the prosthetic heme group to bind O₂ and serves to regulate the O₂ binding affinity.

On the basis of the crystal structure of the HSA–heme complex, we have used site-directed mutagenesis to introduce into the heme binding site of HSA a histidine that would be predicted to provide axial coordination to the central Fe²⁺ atom of the heme and thereby promote O₂ binding (Figure 1). An initial recombinant HSA mutant, in which Ile-142 and Tyr-161 were replaced by His and Leu, respectively [rHSA(I142H/Y161L)], has been made, and the O₂ binding capabilities of the heme complex have been partially evaluated.¹¹ In the present study, we have elucidated the coordination structure of the naturally occurring wild-type rHSA–heme [rHSA(wt)–heme] by UV–vis and magnetic circular dichroism (MCD) spectroscopies and characterized the unusual axial coordination of Tyr-161 to the heme. To develop HSA–heme as a synthetic O₂ carrier, we have also generated several new mutant rHSA–heme complexes. Their O₂ and CO binding properties have been characterized kinetically and compared to those of the natural Hb, Mb, and recombinant Mb (rMb) mutants. We have shown

that our mutagenesis approach can create a new class of albumin-based artificial hemoproteins which would serve as an O₂ carrier.

Experimental Section

Materials and Apparatus. rHSA(wt) was kindly provided by the NIPRO Corp. (Osaka, Japan). All reagents were purchased from commercial sources as special grades and used without further purification unless otherwise noted. Iron(III) protoporphyrin IX (hemin) chloride was purchased from Fluka. Horse skeletal muscle myoglobin (Mb) was purchased from Sigma-Aldrich. The iron(III) protoporphyrin IX dimethyl ester chloride (FePPIXDME) was prepared by esterification of carboxylate side chains of hemin with acidic methanol. The UV–vis absorption spectra were recorded using an Agilent 8453 UV–visible spectrophotometer fitted with an Agilent 89090A temperature control unit.

Site-Directed Mutagenesis, Protein Expression, and Purification. Specific mutations were introduced into HSA within the context of a plasmid vector containing the entire HSA coding region (pHIL-D2 HSA) using designed primers with the QuikChange XL site-directed mutagenesis kit (Stratagene).¹³ All mutations were confirmed by DNA sequencing. Each mutated pHIL-D2 HSA plasmid was linearized by NotI digestion and introduced into *Pichia pastoris* GS115 by electroporation using a BioRad MicroPulser. Expressions were carried out by standard protocols (Invitrogen) with some modifications. Clones were grown upon BMGY medium [1% yeast extract, 2% peptone, 0.1 M potassium phosphate (pH 6.0), 1.34% yeast nitrogen base without amino acids, 40 ppm biotin, 1% glycerol] and transferred to BMMY medium [1% yeast extract, 2% peptone, 0.1 M potassium phosphate (pH 6.0), 1.34% yeast nitrogen base without amino acids, 40 ppm biotin, 1% methanol] for induction with methanol in baffled shaking flasks at 30 °C in a JEIOTECH SI-600R incubator at 200 rpm.

(10) Marden, M. C.; Hazard, E. S.; Leclerc, L.; Gibson, Q. H. *Biochemistry* **1989**, *28*, 4422–4426.

(11) Komatsu, T.; Ohmichi, N.; Zunszain, P. A.; Curry, S.; Tsuchida, E. *J. Am. Chem. Soc.* **2004**, *126*, 14304–14305.

(12) The pictures were produced on the basis of crystal structure coordinate of the rHSA(wt)–heme (code: 1O9X, ref 3e) using PyMOL. DeLano, W. L. The PyMOL Molecular Graphics System 2002 DeLano Scientific, San Carlos, CA.

(13) (a) Peterson, C. E.; Ha, C.-E.; Jameson, D. M.; Bhagavan, N. V. *J. Biol. Chem.* **1996**, *271*, 19110–19117. (b) Peterson, C. E.; Ha, C.-E.; Harohalli, K.; Park, D.; Bhagavan, N. V. *Biochemistry* **1997**, *36*, 7012–7017.

The secreted rHSA was isolated as follows. The growth medium was centrifuged to harvest the culture supernatant, which was brought to 50% saturation by the addition of solid ammonium sulfate with stirring at room temperature. The mixture was then incubated at 4 °C for 1 h. The resulting precipitate was removed by centrifugation, and the supernatant fluid was brought to 95% saturation with ammonium sulfate. The precipitated protein, which contains rHSA, was collected by centrifugation and dissolved in distilled water. The brownish solution was dialyzed for 48 h at 4 °C against 100 volumes of distilled water, followed by 24 h against 100 volumes of 50 mM potassium phosphated buffer (pH 7.0). The dialysate was then loaded onto a Cibacron Blue column of Blue Sepharose 6 Fast Flow (Amersham Pharmacia Biotech) and washed with 10 bed volumes of 50 mM potassium phosphate. Elution of the rHSA(mutant) was carried out with 3 M NaCl and the eluent dialyzed against 50 mM potassium phosphate. After concentration using an ADVANTEC Q0100 ultrafilter (10 kDa Mw cutoff) in an UHP-43K ultraholder, the samples were applied to a Superdex 75 column (Amersham Pharmacia Biotech) using 50 mM potassium phosphate as the running buffer. All the purification steps were followed by SDS-PAGE analysis. Each rHSA(mutant) exhibited a single band and migrated the same distance as rHSA(wt). The protein concentration was assayed by measuring the absorbance at 280 nm ($\epsilon_{280} = 3.4 \times 10^4 \text{ M}^{-1} \text{ cm}^{-1}$).

Preparations of rHSA-Hemin and rHSA-Heme Complexes. The ferric rHSA(mutant)-hemin complexes were prepared according to our previously reported procedures for rHSA(wt)-hemin.^{3c} Typically 5 mL of 0.1 mM rHSA(mutant) in 50 mM potassium phosphate (pH 7.0) was mixed with 0.8 mL of 0.688 mM hemin in DMSO [hemin:rHSA-(mutant) molar ratio of 1.1] and incubated overnight with rotation in the dark at room temperature. The complex was then diluted with 50 mM potassium phosphate (200 mL) and concentrated to the initial volume (5.8 mL) using an ADVANTEC Q0100 ultrafilter (10 kDa Mw cutoff). These dilution and concentration cycles were repeated to reduce the final concentration of DMSO to <0.1 vol %. The resulting samples were analyzed by a SDS-PAGE to confirm the protein integrity and concentration.

The 50 mM phosphate-buffered solution (pH 7.0) of rHSA(mutant)-hemin ([hemin] = ca. 10 μM) in a 10 mm path length optical quartz cuvette sealed with a rubber septum was purged with Ar for 40 min. A small excess amount of degassed aqueous sodium dithionate was added by microsyringe to the sample under an Ar atmosphere to reduce the central ferric ion of the hemin, generating the deoxy ferrous rHSA-(mutant)-heme complexes.

Kinetic Measurements for O₂ and CO Bindings. Kinetics studies were carried out using laser flash photolysis techniques at 22 °C, except for the determination of the CO dissociation rates. Laser flash photolysis experiments were performed using a Unisoku TSP-1000WK time-resolved spectrophotometer with a Spectron Laser Systems SL803G-10 Q-switched Nd:YAG laser, which generated a second-harmonic (532 nm) pulse of 6 ns duration (10 Hz). The probe light from a 150 W xenon arc-lamp was passed through an UV cutoff filter and an Asahi Spectra MC filter before irradiation to minimize any sample damage. Normally, fresh solutions of the deoxy rHSA(mutant)-heme were made up for each set of experiments, and the gas mixture with the desired partial pressure of O₂/CO/N₂ prepared by a KOFLOC Gasblender GB-3C was flowed into the sample cuvette for 20 min for equilibration.

In general, recombination following laser flash photolysis to hemeO₂ or hemeCO occurs according to eq 1 with the association rate constant (k_{on}^{L}), dissociation rate constant ($k_{\text{off}}^{\text{L}}$), and apparent rate constant (k_{app}) given by eq 2.^{14,15} The values of k_{app} were obtained directly from the log plots of the change in absorbance (ΔA) versus time. The gas



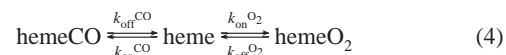
$$k_{\text{app}} = k_{\text{on}}^{\text{L}}[\text{L}] + k_{\text{off}}^{\text{L}} \quad (2)$$

concentrations were always higher than that of the heme; therefore, the pseudo-first-order approximation can be applied throughout. For CO rebinding at high [CO], eq 2 reduces to eq 3 because $k_{\text{on}}^{\text{CO}}[\text{CO}] \gg k_{\text{off}}^{\text{CO}}$.

$$k_{\text{app}} \approx k_{\text{on}}^{\text{CO}}[\text{CO}] \quad (3)$$

Thus, $k_{\text{on}}^{\text{CO}}$ of the rHSA(mutant)-heme was easily calculated from $k_{\text{app}}/[\text{CO}]$.

The O₂ association rates ($k_{\text{on}}^{\text{O}_2}$) and the O₂ binding constants [$K^{\text{O}_2} = (P_{1/2}^{\text{O}_2})^{-1}$] of the rHSA(mutant)-heme were measured using the competitive rebinding technique.^{14,15} Photolysis of hemeCO in the presence of CO and O₂ gives the five-*N*-coordinate heme (deoxy state), which is first trapped as hemeO₂ and subsequently converted back to hemeCO (eq 4).



The CO concentration was held constant, and the fast and slow kinetics were measured at different [O₂]. The fast process is given by eq 5, allowing the direct determination of $k_{\text{on}}^{\text{O}_2}$ from a plot of $k_{\text{app}}(\text{fast})$ versus [O₂].

$$k_{\text{app}}(\text{fast}) = k_{\text{on}}^{\text{O}_2}[\text{O}_2] + k_{\text{off}}^{\text{O}_2} + k_{\text{on}}^{\text{CO}}[\text{CO}] \quad (5)$$

The rate constant for the slower process, $k_{\text{app}}(\text{slow})$, is substituted into Traylor's eq 6 to obtain $K^{\text{O}_2} [(P_{1/2}^{\text{O}_2})^{-1}]$.¹⁵

$$\frac{k_{\text{on}}^{\text{CO}}[\text{CO}]}{k_{\text{app}}(\text{slow})} = K^{\text{O}_2}[\text{O}_2] + \frac{k_{\text{on}}^{\text{CO}}[\text{CO}]}{k_{\text{off}}^{\text{O}_2}} + 1 \quad (6)$$

The value of $k_{\text{on}}^{\text{CO}}[\text{CO}]$ is constant; therefore, the plots of $k_{\text{on}}^{\text{CO}}[\text{CO}]/k_{\text{app}}(\text{slow})$ versus [O₂] affords K^{O_2} .

The relaxation curves that accompanied the O₂ or CO recombination were fitted to single- or double-exponentials using the Unisoku Spectroscopy & Kinetics Software. The $k_{\text{off}}^{\text{O}_2}$ values can be determined from the y-intercept of eq 5 or 6, but they often have large deviations. Therefore, we calculated $k_{\text{off}}^{\text{O}_2}$ from $k_{\text{on}}^{\text{O}_2}/K^{\text{O}_2}$ (both obtained from slopes).

The CO dissociation from the rHSA(mutant)-hemeCO was measured by carrying out the replacement reaction with NO.¹⁶ A Sephadex G-25 column was equilibrated with CO-saturated potassium phosphate buffer (50 mM, pH 7.0), and the rHSA(mutant)-hemeCO solution was passed through the column to remove the dithionate. The eluent was directly connected to a optical quartz cuvette under a 10% CO (in N₂) atmosphere. The 10% NO (in N₂) equilibrated buffer was then rapidly injected into the rHSA(mutant)-hemeCO solution, and the time dependence of the decrease in absorption at 418 nm was monitored. The relaxation curves that accompanied the CO dissociation within several minutes were analyzed by fitting to double-exponentials. The CO binding constants [$K^{\text{CO}} = (P_{1/2}^{\text{CO}})^{-1}$] were calculated using $k_{\text{on}}^{\text{CO}}/k_{\text{off}}^{\text{CO}}$.

Magnetic Circular Dichroism (MCD). The MCD for the 50 mM potassium phosphate-buffered solutions (pH 7.0) of the rHSA(wt)-heme and rHSA(mutant)-heme series (8.0 μM) under Ar and CO atmospheres were measured using a JASCO J-820 circular dichrometer fitted with a 1.5 T electromagnet at 22 °C. The spectrum was acquired five times to improve signal-to-noise, and each data point was corrected

(14) Collman, J. P.; Brauman, J. I.; Iverson, B. L.; Sessler, J. L.; Moris, R. M.; Gibson, Q. H. *J. Am. Chem. Soc.* **1983**, *105*, 3052–3064.

(15) Traylor, T. G.; Tsuchiya, S.; Campbell, D.; Mitchel, M.; Styne, D.; Koga, N. *J. Am. Chem. Soc.* **1985**, *107*, 604–614.

(16) Rohlfis, R.; Mathews, A. J.; Carver, T. E.; Olson, J. S.; Springer, B. A.; Egeberg, K. D.; Slinger, S. G. *J. Biol. Chem.* **1990**, *265*, 3168–3176.

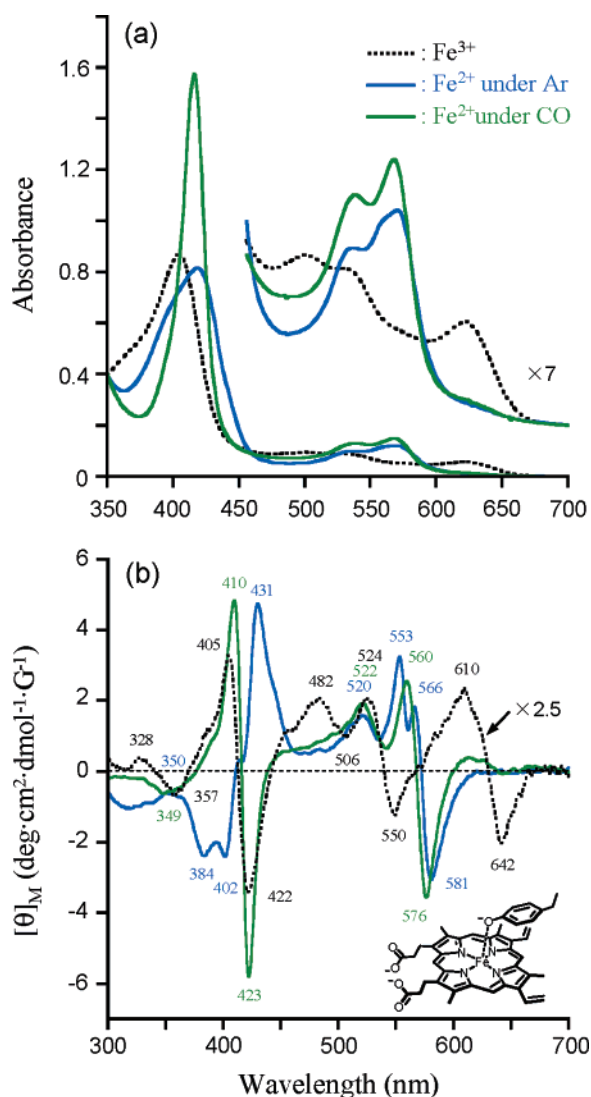


Figure 2. (a) UV-vis absorption and (b) MCD spectral changes of the rHSA(wt)-heme in 50 mM potassium phosphate buffered solution (pH 7.0, 22 °C).

by subtracting the optical rotation observed in the absence of an applied magnetic field.

Results and Discussion

Naturally Occurring rHSA(wt)-Hemin. Our crystal structure analysis revealed that heme is bound within a D-shaped cavity in subdomain IB of rHSA(wt), where the central ferric ion is coordinated by Tyr-161, and the two propionate side chains are coordinated by a triad of basic amino acid residues (Figure 1).^{3c} The UV-vis absorption spectrum of the phosphate-buffered solution (50 mM, pH 7.0) of rHSA(wt)-hemin showed a Soret band at 405 nm and the charge-transfer (CT) band of the porphyrin $\rho\pi$ to the Fe^{3+} $d\pi$ orbitals at 624 nm (Figure 2a). The spectral pattern and amplitudes were almost constant in the temperature range of 5–40 °C. The dominant feature of the spectrum was quite similar to those of the human or horse heart ferric H93Y recombinant Mb [rMb(H93Y)], in which the proximal histidine (His-93) was replaced with Tyr by site-directed mutagenesis (Table 1).^{17,18} Adachi and co-workers showed that the ferric rMb(H93Y) formed a five-coordinate high-spin complex with a single oxygen donor of the proximal

Table 1. UV-vis Absorption Spectral Data of the rHSA(wt)-Heme, rHSA(mutant)-Heme and Other Hemoproteins

Hemoproteins	State	λ_{max} (nm)	
		Soret	Visible
rHSA(wt)-Heme ^a	Fe^{3+}	405	501, 534, 624
	Fe^{2+}	419	538, 559(sh), 570
	Fe^{2+}CO	416	539, 568
HSA-Heme ^b	Fe^{3+}	404	498, 530, 620
	Fe^{2+}	416	534, 570
	Fe^{2+}CO	418	536, 568
Human rMb(H93Y) ^c	Fe^{3+}	402	480, 520(sh), 598
	Fe^{2+}	427	560
	Fe^{2+}CO	420	539, 567
Horse Heart rMb(H93Y) ^d	Fe^{3+}	403	487, 524, 599
	Fe^{2+}	429	556
	Fe^{2+}CO	419	539, 570
FePPIXDME(CH_3O^-) ^e	Fe^{3+}	401	476, 580(sh), 600
FePPIXDME($p\text{-NO}_2\text{PhO}^-$) ^f	Fe^{3+}	402	500, 528, 621
FePPIXDME ^{a,g}	Fe^{3+}	400	571, 599
	Fe^{2+}	393, 414, 427, 440(sh)	535, 571
rHSA(I142H)-Heme ^a	Fe^{2+}CO	411	532, 564
	Fe^{3+}	404	501, 533, 619
	Fe^{2+}	424	530, 558
rHSA(I142H/Y161L)-Heme ^a	Fe^{2+}CO	419	537, 560
	Fe^{3+}	402	533, 620
	Fe^{2+}	426	531(sh), 559
rHSA(I142H/Y161Y)-Heme ^a	Fe^{2+}O_2	412	537, 573
	Fe^{2+}CO	419	538, 565
	Fe^{3+}	402	533, 620
rHSA(Y161L/L185H)-Heme ^a	Fe^{2+}	425	532(sh), 559
	Fe^{2+}O_2	411	538, 576
	Fe^{2+}CO	419	538, 565
Mb ^{a,h}	Fe^{3+}	408	528, 620
	Fe^{2+}	422	530, 558
	Fe^{2+}O_2	412	538, 570
	Fe^{2+}CO	419	537, 560
	Fe^{3+}	409	503, 548(sh), 632
	Fe^{2+}	434	557
	Fe^{2+}O_2	418	544, 581
	Fe^{2+}CO	423	541, 579

^a In 50 mM potassium phosphate buffer (pH 7.0, 22 °C). ^b In 0.1 M phosphate buffer (pH 7.0); ref 22. ^c In 50 mM sodium phosphate buffer (pH 7.0, 20 °C); ref 17. ^d At pH 7–10, 25 °C; ref 18. ^e In $\text{CH}_2\text{Cl}_2/\text{CH}_3\text{OH} = 9/1$ (v/v) (25 °C); ref 21. ^f In CH_2Cl_2 (25 °C); ref 21. ^g In 0.5% Me_3CnBr . ^h Horse muscle Mb (Sigma).

Tyr-93 by resonance Raman spectroscopy.^{17b} Our absorption spectral data imply that the heme is bound to Tyr-161 of rHSA(wt) and forms a ferric five-coordinate high-spin complex under physiological conditions. Interestingly, the CT absorptions of the rHSA(wt)-hemin appeared at a higher wavelength ($\lambda_{\text{max}} = 624$ nm) compared to rMb(H93Y) ($\lambda_{\text{max}} = 598\text{--}599$ nm). Dawson and co-workers classified the CT bands of the oxygen-ligated hemins into two groups: the first at around 600 nm for rMb(H93Y) and the methoxide (CH_3O^-) complex of Fe^{3+} protoporphyrin IX dimethyl ester ($\text{Fe}^{3+}\text{PPIXDME}$), and the second at around 620 nm for p -nitrophenolate ($p\text{-NO}_2\text{PhO}^-$) or the acetate complex of $\text{Fe}^{3+}\text{PPIXDME}$, in which the nonoccupied π^* orbitals of the fifth ligand interacts with the Fe^{3+} $d\pi$ orbitals and, in turn, lowered the energy level of the CT transition (Table 1).¹⁹ The rHSA(wt)-hemin definitely belongs to the latter group, which suggests that the axial coordination

- (17) (a) Adachi, S.; Nagano, S.; Watanabe, Y.; Ishimori, K.; Morishima, I. *Biochim. Biophys. Res. Commun.* **1991**, *180*, 138–144. (b) Adachi, S.; Nagano, S.; Ishimori, K.; Watanabe, Y.; Morishima, I.; Egawa, T.; Kitagawa, T.; Makino, R. *Biochemistry* **1993**, *32*, 241–252.
(18) Hildebrand, D. P.; Burk, D. L.; Maurus, R.; Ferrer, J. C.; Brayer, G. D.; Mauk, A. G. *Biochemistry* **1995**, *34*, 1997–2005.
(19) Pond, A. E.; Roach, M. P.; Sono, M.; Rux, A. H.; Franzen, S.; Hu, R.; Thomas, M. R.; Wilks, A.; Dou, Y.; Ikeda-Saito, M.; Ortiz de Montellano, P. R.; Woodruff, W. H.; Boxer, S. G.; Dawson, J. H. *Biochemistry* **1999**, *38*, 7601–7608.

of Tyr-161 to the heme is weaker than that of rMb(H93Y) and Fe³⁺PPIXDME(CH₃O⁻). This is consistent with the observation that the Fe³⁺-O(phenolate) distance in the crystal structure of the rHSA(wt)-hemin (2.78 Å) is greater than that for rMb(H93Y) (1.91 Å).^{3e}

We then employed MCD spectroscopy to elucidate the axial coordination environment of the rHSA(wt)-hemin. MCD is a powerful probe of the oxidation state, spin state, and the nature of the axial ligand in heme system and has frequently been used as a method of comparison between synthetic iron porphyrins of known axial ligation and newly discovered hemoproteins of unknown ligation.²⁰ The ferric rHSA(wt)-hemin showed a characteristic MCD pattern with two distinct troughs in the visible region (550, 642 nm) (Figure 2b), which was more similar to that of the five-coordinate Fe³⁺PPIXDME (*p*-NO₂-PhO⁻) than to that of the Fe³⁺PPIXDME(CH₃O⁻).^{19,21} The MCD of the rHSA(wt)-hemin therefore also supports the formation of a five-coordinate high-spin heme complex with weak axial ligation by Tyr-161.

Reduced Ferrous rHSA(wt)-Heme. Reduction of the ferric rHSA(wt)-hemin by the addition of sodium dithionate under an Ar atmosphere gave a ferrous heme complex with a broad Soret band at 419 nm ($\Delta\lambda_{1/2} = 61$ nm) and two definite Q-bands at 538 and 570 nm (Figure 2a). This is in significant contrast to human ferrous rMb(H93Y) in a five-coordinate high-spin complex, which exhibits a similar spectrum to deoxy Mb with a sharp Soret band and single Q-band absorption around 560 nm (Table 1).^{17,18} The shoulder at 559 nm in the spectrum of the rHSA(wt)-heme is probably due to a ferrous five-coordinate complex, but this clearly coexists with another species. One possible candidate is a six-coordinate low-spin complex. Casella and co-workers proposed that the reduced HSA-heme contains a six-coordinate heme.²² Nevertheless, the MCD spectrum of the ferrous rHSA(wt)-heme (Figure 2b) was quite different from the well-known shape of the six-coordinate low-spin heme derivatives, such as cytochrome *b*₅ and bisimidazole-ligated Fe²⁺PPIXDME, which show a sharp and intense Faraday A term corresponding to the α band.^{20c}

Another possibility is a four-coordinate intermediate spin state ($S = 1$) not found in natural Mb. Phosphate-buffered solutions (pH 7.0) of 0.5% (w/v) *N*-cetyltrimethylammonium bromide (CetMe₃NBr) micelles containing dissolved Fe²⁺PPIXDME showed a multiple broad Soret band ($\Delta\lambda_{1/2} = 73$ nm) and well-defined β and α bands (535 and 571 nm) (Table 1, see Figure S1a), a spectral pattern consistent with a four-coordinate Fe²⁺-mesoporphyrin IX dimethyl ester in the CetMe₃NBr suspension.²³ This observation suggests that the strong β and α bands (538, 570 nm) in the UV-vis absorption spectrum of the rHSA(wt)-heme complex also derived from a ferrous four-coordinate complex. The micellar solution of Fe²⁺PPIXDME showed

complicated MCD bands in the Soret region and two positive peaks (522, 562 nm) and one trough (579 nm) in the visible region (see Figure S1b). The typical MCD of five-coordinate deoxy Mb is shown in Figure 4b (vide infra). Comparison of these data with the MCD spectral pattern of ferrous rHSA(wt)-heme suggests that the latter involves both important features of four- and five-coordinate heme complexes (Figure 2b). Therefore, we conclude that the reduced ferrous rHSA(wt)-heme is in an unusual mixture of a five-coordinate high-spin complex ($S = 5/2$) with Tyr-161 and a four-coordinate intermediate spin state ($S = 1$) under an Ar atmosphere. The estimated ratio of the five- and four-coordinate complexes is approximately 1/1.

Upon the addition of O₂ gas to this solution, the central ferrous ion was rapidly autoxidized even at low temperature (~ 0 °C), and the UV-vis absorption spectrum returned to the initial ferric complex. On the other hand, a carbonyl complex was formed at room temperature and exhibited a very similar absorption ($\lambda_{\text{max}} = 416, 539, 568$ nm) to human and horse rMb(H93Y)CO (Figure 2a, Table 1).^{17,18} The MCD spectrum of the rHSA(wt)-hemeCO showed simple Faraday A terms associated with the porphyrin $\pi-\pi^*$ transitions, which are typical of a low-spin carbonyl heme (Figure 2b).²⁰ The rHSA(wt)-hemeCO could be a diamagnetic low-spin complex with a phenolate ligand (Tyr-161) similar to what was found for rMb(H93Y).

In our blood stream, the most avid carrier of heme is the specific heme-binding protein, hemopexin.^{24,25} The binding constant of hemopexin for heme is 10⁴-fold higher than HSA. However, due to the extremely low abundance of hemopexin in plasma (< 17 μM), HSA acts as a significant depot of heme in the circulation. The heme binding to these proteins not only conserves the porphyrin iron and channels it to the specific catabolism site but it also prevents its toxic effects, such as the catalysis of hydroxyl radical production. Furthermore, HSA-heme exhibits little peroxidase or catalase activities.²² The weak axial coordination of phenolate to HSA-bound heme may therefore have evolved for (1) easy release and transfer to hemopexin in the blood stream, and (2) maintenance of the antioxidative homeostasis in the extracellular fluids of our body.

Genetic Engineered rHSA(mutant) Complexed with Heme. The detailed architecture of the heme-binding site in HSA revealed by our crystallographic studies allows us to design mutagenesis experiments to construct a tailor-made heme pocket for stable O₂ binding. Tyr-161 was the first candidate considered for site-directed mutagenesis to introduce a proximal histidine; however, the Y161H mutation was not done because our simulations indicated that the distance from N_ε(H161) to Fe-(heme) would be too great (4.0 Å). Instead, modeling experiments suggested that the favorable positions for the axial imidazole insertion would be Ile-142 and Leu-185 (Figure 1). The N_ε(histidine)-Fe distances were estimated to be 2.31 Å for H142 and 2.69 Å for H185 (compared to 2.18 Å for Mb). We therefore designed and produced a single mutant I142H and three double mutants I142H/Y161L, I142H/Y161F, and Y161L/L185H (see Experimental Section).

The UV-vis absorption and MCD spectra of the rHSA(I142H/Y161L)-hemin and rHSA(I142H/Y161F)-hemin are

- (20) (a) Collman, J. P.; Basolo, F.; Bunnenberg, E.; Collins, T. J.; Dawson, J. H.; Ellis, P. E., Jr.; Marrocco, M. L.; Moscovitz, A.; Sessler, J. L.; Szymanski, T. *J. Am. Chem. Soc.* **1981**, *103*, 5636–5648. (b) Cheek, J.; Dawson, J. H. *Magnetic Circular Dichroism Spectroscopy of Heme Proteins and Model Systems*. In *The Porphyrin Handbook*; Kadish, K. M., Smith, K. M., Guilard, R., Eds.; Academic Press: San Diego, 2000; Vol. 7, pp 339–369. (c) Svatits, E. W.; Dawson, J. H. *Inorg. Chim. Acta.* **1986**, *123*, 83–86.
- (21) Nozawa, T.; Okubo, S.; Hatano, M. *J. Inorg. Biochem.* **1980**, *12*, 253–267.
- (22) Monzani, E.; Bonafè, B.; Fallarini, A.; Redaelli, C.; Casella, L.; Minchiotti, L.; Galliano, M. *Biochim. Biophys. Acta* **2001**, *1547*, 302–312.
- (23) Geibel, J.; Cannon, J.; Campbell, D.; Traylor, T. G. *J. Am. Chem. Soc.* **1978**, *100*, 3575–3585.

- (24) Tolosano, E.; Altruda, F. *DNA Cell Biol.* **2002**, *21*, 297–306.
- (25) Paoli, M.; Anderson, B. F.; Baker H. M.; Morgan, W. T.; Smith, A.; Baker, E. N. *Nat. Struct. Biol.* **1999**, *6*, 926–931.

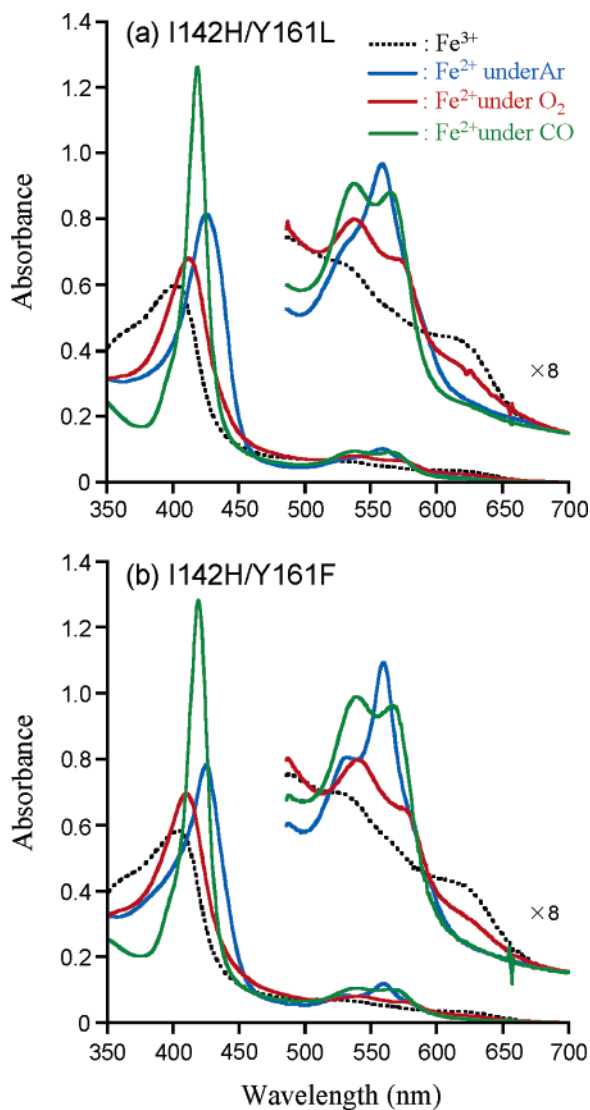


Figure 3. UV-vis absorption spectral changes of the (a) rHSA(I142H/Y161L)-heme and (b) rHSA(I142H/Y161F)-heme in 50 mM potassium phosphate buffered solution (pH 7.0, 8 °C).

essentially the same in their general features (Figure 3 and Figure S2). The strong absorption band due to the porphyrin-to-metal CT was weakened because of the Y161L and Y161F mutations (Figure 3). Both MCD spectra showed similar S-shaped patterns in the Soret band region, which resembled that of ferric Mb (see Figure S2).²⁶ It is known that two water molecules are located in the heme pocket of ferric Mb.²⁷ One water axially coordinates to the sixth position of the central ferric ion of the heme to produce the aquo complex, and the other one is at the rear of the pocket, hydrogen bonded to the first water. A great number of MCD studies on synthetic iron porphyrins and hemoproteins have demonstrated that the spectral shape in the Soret region can be used as a qualitative marker of the spin state and axial coordination environment.²⁰ Vickery and co-workers found that (i) the Soret MCD intensity of the ferric Mb with different anions at the six-coordinate position was correlated with the amount of low-spin component formed,

(26) Vickery, L.; Nozawa, T.; Sauer, K. *J. Am. Chem. Soc.* **1976**, *98*, 343–350.

(27) Springer, B. A.; Sligar, S. G.; Olson, J. S.; Phillips, G. N., Jr. *Chem. Rev.* **1994**, *94*, 699–714.

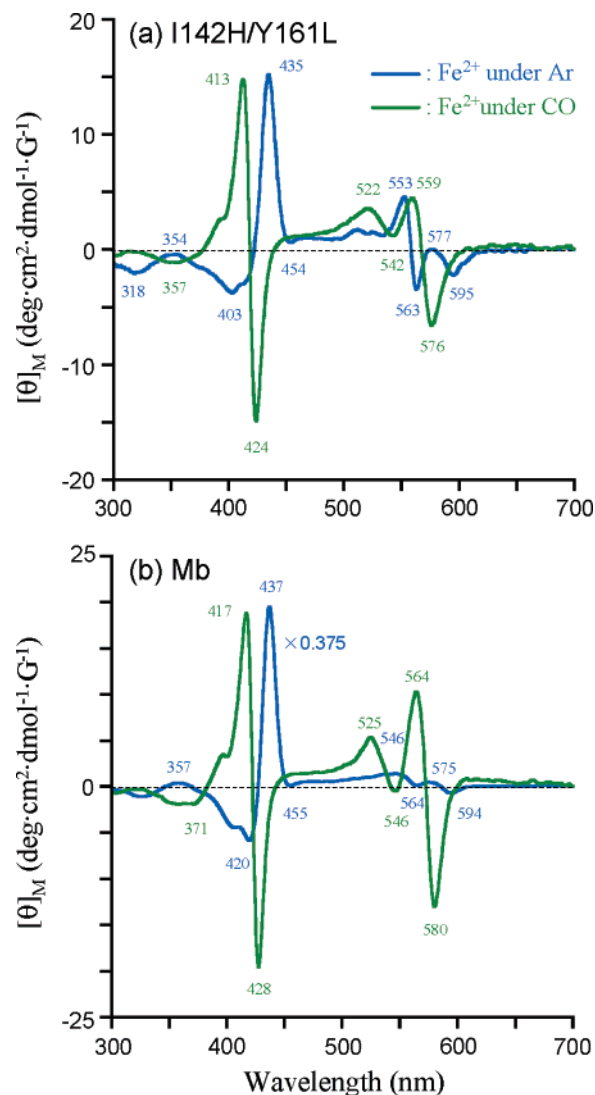


Figure 4. MCD spectral changes of the (a) rHSA(I142H/Y161L)-heme and (b) native Mb in 50 mM potassium phosphate buffered solution (pH 7.0, 22 °C).³⁰

and (ii) the shape of the band is sensitive to the nature of the sixth ligand.²⁶ Our MCD results suggest that both the rHSA(I142H/Y161L)-heme and rHSA(I142H/Y161F)-heme are in predominantly ferric high-spin complexes having a water molecule as the sixth ligand.

O₂ and CO Binding to Ferrous rHSA(mutant)-Heme. The rHSA(mutant)-heme was easily reduced to the ferrous complex by adding a small molar excess of aqueous sodium dithionite under an Ar atmosphere. A single broad absorption band ($\lambda_{\text{max}} = 559$ nm) in the visible region of the rHSA(I142H/Y161L)-heme and rHSA(I142H/Y161F)-heme was similar to that observed for deoxy Mb²⁸ or the chelated heme in DMF,²⁹ indicating the formation of a five-*N*-coordinate high-spin complex (Figure 3, Table 1). The spectral features and amplitude were unaltered in the temperature range of 0–25 °C. The heme therefore appears to be accommodated in the mutated heme pocket with an axial coordination involving His-142. Upon exposure of the rHSA(I142H/Y161L)-heme and rHSA(I142H/

(28) Antonini, E.; Brunori, M. *Hemoglobin and Myoglobin in Their Reactions with Ligands*; North-Holland Pub.: Amsterdam, 1971; p 18.

(29) Traylor, T. G.; Chang, C. K.; Geibel, J.; Berzins, A.; Mincey, T.; Cannon, J. *J. Am. Chem. Soc.* **1979**, *101*, 6716–6731.

Y161F)–heme solutions to O₂, the UV–vis absorptions immediately changed to that of the O₂ adduct complex at 0–25 °C (Figure 3).^{28,29} After flowing CO gas, these hemoproteins produced stable carbonyl complexes.

The MCD spectra of the deoxy and carbonyl rHSA(I142H/Y161L)–heme are shown in Figure 4a. The Soret MCD of the deoxy state under anaerobic conditions is dominated by an intense positive peak at 435 nm, as would be expected for the Faraday *C* terms anticipated for the high-spin Fe²⁺ porphyrin.^{20a,26} On the other hand, the rHSA(I142H/Y161L)CO exhibited S-shaped MCDs which correspond to the *A* term bands for the diamagnetic Fe²⁺ porphyrin.^{20a,26} These spectra are very similar to those of the high-spin deoxy Mb and low-spin MbCO measured in identical conditions (Figure 4b). Our MCD results clearly show that the central ferrous ion of the heme is coordinated by His-142 in the heme pocket and forms a five-*N*-coordinate high-spin complex under an Ar atmosphere, which converts to the low-spin diamagnetic form by the binding of CO. The rHSA(I142H/Y161L)–heme complex had the same MCD spectral features as rHSA(I142H/Y161L)–heme (data not shown).

The single mutant rHSA(I142H)–heme complex, which retains Y161, could not bind O₂. The polar phenolate residue at the top of the porphyrin plane is likely to accelerate the proton-driven oxidation of the Fe²⁺ center. This rapid autoxidation is also observed in the rMb(H64Y) mutants, in which the distal histidine (His-64) was substituted with Tyr, thus introducing a potentially anionic nucleophile near to the O₂ coordination site.³¹ In contrast, replacement of Tyr-161 in rHSA(I142H)–heme by Leu or Phe enhanced the stabilization of the O₂ adduct complex. In the rHSA(Y161L/L185H)–heme, the proximal histidine coordinated to the central ferrous ion from the opposite side of the porphyrin platform also allows O₂ binding to the heme. The lifetimes for the decays of the dioxygenated rHSA(I142H/Y161L)–heme, rHSA(I142H/Y161F)–heme, and rHSA(Y161L/L185H)–heme are all 3–5 min at 20 °C.

To evaluate the kinetics of the O₂ and CO bindings to the rHSA(mutant)–heme, laser flash photolysis experiments were carried out.^{14,15} The transient absorption spectra of the photodissociated product of the rHSA(I142H/Y161L)–hemeCO displayed a negative absorbance at 417 nm, due to the disappearance of the carbonyl complex, and a positive absorbance at 435 nm, which is attributed to the deoxy form (Figure 5). The transient absorption spectra in the time range from 0.1 μs to 8.0 ms with an isosbestic point at 401, 426, and 458 nm were superimposed on the static difference spectrum of the deoxy minus carbonyl compound (Figure 5, red line). They illustrate the process of reassociation of CO and are consistent with the formation of the ferrous five-*N*-coordinate high-spin complex after the laser pulse irradiation.

It is noteworthy that the absorbance decays accompanying the CO recombinations to these rHSA(mutant)–heme were composed of double-exponential profiles, which are normally not observed in Mb (Figure 6a). The ratio of the amplitude of the fast and slow phases was approximately 3:2 for the rHSA(I142H/Y161L)–heme, 5:1 for the rHSA(I142H/Y161F)–heme and 3:1 for the rHSA(Y161L/L185H)–heme. On the other hand,

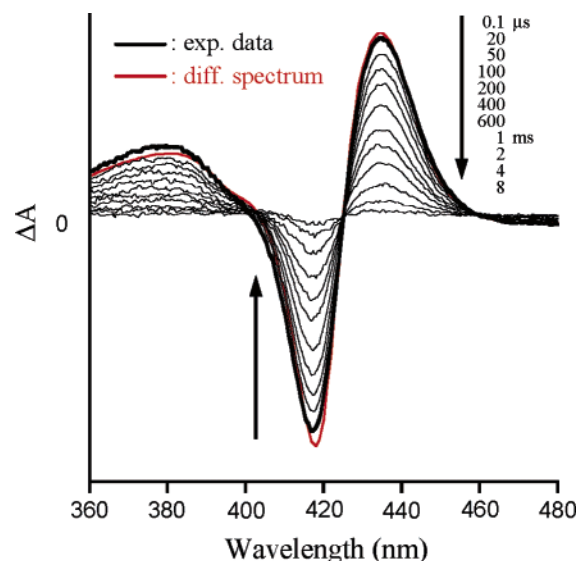


Figure 5. Transient absorption spectra of the photodissociated product of the rHSA(I142H/Y161L)–hemeCO after the laser flash photolysis at 22 °C. The red-line represents the static spectrum of deoxy minus carbonyl compound in Figure 3a.

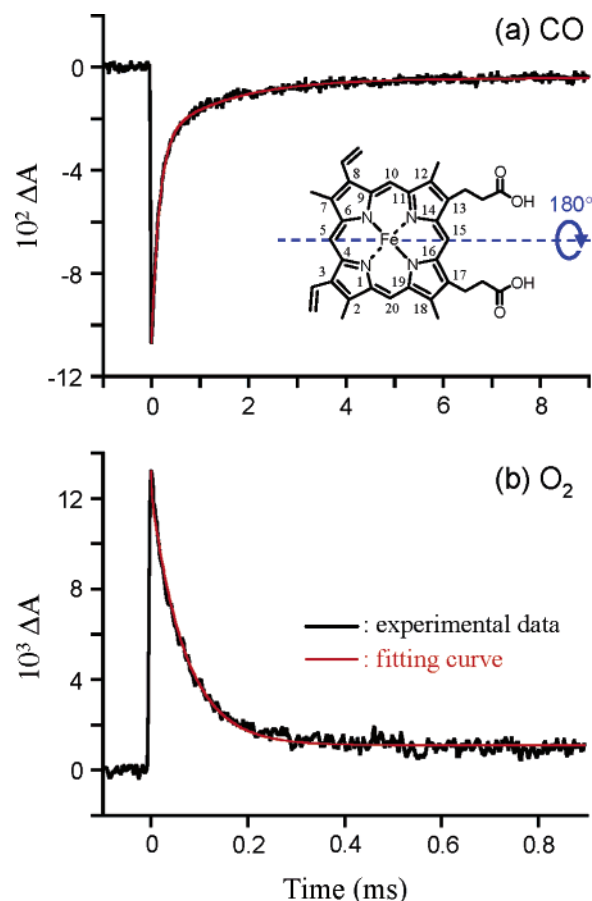


Figure 6. Absorption decay of CO rebinding to the rHSA(I142H/Y161F)–heme after the laser flash photolysis at 22 °C; the kinetics was composed of two phases and relaxation curve was fitted by double-exponentials. (b) Absorption decay of O₂ rebinding to the rHSA(I142H/Y161F)–heme after the laser flash photolysis at 22 °C; the kinetics was fitted by single-exponential relaxation curve.

the rebinding of O₂ to the rHSA(mutant)–heme followed a simple monophasic decay (Figure 6b). From numerous investigations on synthetic model hemes, it has been shown that a bending

(30) The spectra of Mb are consistent with other results reported elsewhere; refs 20, 26.

(31) Springer, B. A.; Egeberg, K. D.; Sliger, S. G.; Rohlfis, R. J.; Mathews, A. J.; Olson, J. S. *J. Biol. Chem.* **1989**, *264*, 3057–3060.

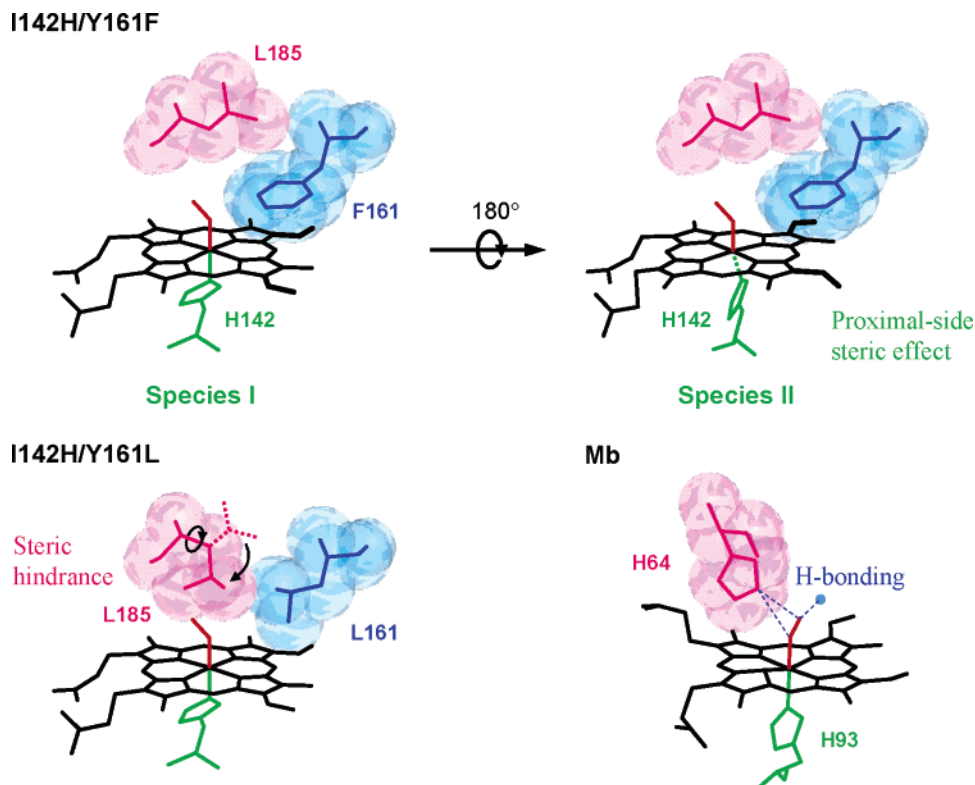


Figure 7. Structural models of the hemeO₂ sites of rHSA(I142H/Y161F)-heme and rHSA(I142L/Y161L)-heme, and comparison to Mb.^{12,32}

strain in the proximal base coordination to the central Fe²⁺ atom, the “proximal-side steric effect”, can both increase the dissociation rate and decrease the association rate for CO, whereas it increases the O₂ dissociation rate without greatly altering the kinetics of O₂ association.^{14,15} One possible explanation is that there may be two different geometries of the axial histidine (His-142 or His-185) coordination to the central ferrous ion of the heme, each one accounting for a component of the biphasic kinetics of CO rebinding. Marden and co-workers also reported a similar two-phase kinetics in CO association with HSA-heme and interpreted it as indicating that there are two different orientations of the porphyrin ring in a single site on HSA.¹⁰ In our case, the alternative geometries may arise because crystallographic analysis suggests that the heme molecule appears able to bind into the narrow cavity of subdomain IB in two orientation that are related by a 2-fold rotation about the 5,15-*meso* axis of the heme (180° rotational isomers). It appears that the asymmetric hydrophobic 3,8-divinyl groups at the porphyrin periphery may occupy different positions that result in a shift of the Fe²⁺ center, forming the two different geometries of the axial imidazole coordination of histidine (Figure 7).

In general, the crystal structures of natural hemoproteins have shown that the prosthetic heme group is bound in a single orientation. On the other hand, in solution, ¹H NMR spectra frequently exhibit two sets of heme (or hemin) resonances, which arise from alternative orientations of the porphyrin plane.³³ This orientational disorder is most readily detected in the ferric low-spin state, which shows extraordinary porphyrin

2,7,12,18-CH₃ contact shifts.³⁴ The amount of the minor species ranges from a few percent in Mb to 40% in insect Hb (*CTT* HbIII).³⁵ Reconstitution techniques have made significant contributions to clarify this molecular equilibrium; the heme in Hb and Mb can be easily removed under acidic conditions and the resulting apoprotein may be reconstituted by adding back the heme to produce the holoprotein.³⁶ The incorporation of hemin into apoMb is complete within 1 ms, but the initial complex does not distinguish the two possible orientations of the porphyrin ring.³⁴ As a result, freshly reconstituted Mb contains an equimolar 1/1 mixture of the two conformers; subsequent heme rearrangement is extremely slow (≈13 h). The influence of the heme orientation on the functional properties appears to be very dependent on the particular protein. In *CTT* HbIII, the O₂ binding affinity depends on the heme orientation.³⁷ On the other hand, the equilibrium and kinetic parameters for O₂ and CO binding to the reconstituted human Mb are unaffected by the slow heme rearrangement.^{38,39}

Our attempts to determine the ratio of the two hemin orientations of the rHSA(I142H/Y161L)-hemin by ¹H NMR spectroscopy unfortunately failed. The downfield spectra of the

(32) The model of Mb was prepared on the basis of crystal structure coordinate of MbO₂ (code: 1MBO, Phillips, S. E. *J. Mol. Biol.* **1980**, *142*, 531–554.). The coordinated O₂ shows a hydrogen bond with N_ε(His-64) and hydrogen bond network through H₂O (light-blue circle) within the distal pocket.

- (33) La Mar, G. N.; Satterlee, J. D.; de Ropp, J. S. Nuclear Magnetic Resonance of Hemoprotein. In *The Porphyrin Handbook*; Kadish, K. M., Smith, K. M., Guilard, R., Eds.; Academic Press: San Diego, 2000; Vol. 5, pp 185–298.
- (34) (a) Jue, T.; Krishnamoorthi, R.; La Mar, G. N. *J. Am. Chem. Soc.* **1983**, *105*, 5701–5703. (b) La Mar, G. N.; Toi, H.; Krishnamoorthi, R. *J. Am. Chem. Soc.* **1984**, *106*, 6395–6401.
- (35) (a) La Mar, G. N.; Davis, N. L.; Parish, D. W.; Smith, K. M. *J. Mol. Biol.* **1983**, *168*, 887–896. (b) La Mar, G. N.; Smith, K. M.; Gersonde, K.; Sick, H.; Overcamp, M. *J. Biol. Chem.* **1980**, *255*, 66–70.
- (36) Hayashi, T.; Hisaeda, Y. *Acc. Chem. Res.* **2002**, *35*, 35–43.
- (37) Gersonde, K.; Sick, H.; Overcamp, M.; Smith, K. M.; Parish, D. W. *Eur. J. Biochem.* **1986**, *157*, 393–404.
- (38) Light, W. R.; Rohlf, R. J.; Palmer, G.; Olson, J. S. *J. Biol. Chem.* **1987**, *262*, 46–52.
- (39) Aojula, H. S.; Wilson, M. T.; Morrison, I. G. *Biochem. J.* **1987**, *243*, 205–210.

Table 2. O₂ Binding Parameters of the rHSA(mutant)-Heme in 50 mM Potassium Phosphate Buffer Solution (pH 7.0) at 22 °C^a

Hemoproteins	$k_{\text{on}}^{\text{O}_2}$ ($\mu\text{M}^{-1}\text{s}^{-1}$)	$k_{\text{off}}^{\text{O}_2}$ (m s^{-1})		$P_{1/2}^{\text{O}_2}$ (Torr)	
		I	II	I	II
rHSA(I142H/Y161L)-Heme	7.5	0.22	1.7	18	134
rHSA(I142H/Y161F)-Heme	20	0.10	0.99	3	31
rHSA(Y161L/L185H)-Heme	31	0.20	2.1	4	41
Hb α (R-state) ^b	33 ^c	0.013 ^d		0.24	
Mb ^{e,f}	14	0.012		0.51	
rMb(H64L) ^f	98	4.1		26	
rMb(H64F) ^f	75	10		82	
RBC ^g				8	

^a Number I or II indicates species I or II. ^b Human Hb α -subunit. ^c In 0.1 M phosphate buffer (pH 7.0, 21.5 °C); ref 40. ^d In 50 mM phosphate buffer (pH 7.0, 20 °C); ref 41. ^e Sperm whale Mb. ^f In 0.1 M potassium phosphate buffer (pH 7.0, 20 °C); ref 16. ^g Human red cell suspension. In isotonic buffer (pH 7.4, 20 °C); ref 42.

Table 3. CO Binding Parameters of the rHSA(mutant)-Heme in 50 mM Potassium Phosphate Buffer Solution (pH 7.0) at 22 °C^a

Hemoproteins	$k_{\text{on}}^{\text{CO}}$ ($\mu\text{M}^{-1}\text{s}^{-1}$)		$k_{\text{off}}^{\text{CO}}$ (s^{-1})		$P_{1/2}^{\text{CO}}$ (Torr)	
	I	II	I	II	I	II
rHSA(I142H/Y161L)-Heme	2.0	0.27	0.013	0.079	0.0053	0.24
rHSA(I142H/Y161F)-Heme	6.8	0.72	0.009	0.061	0.0011	0.068
rHSA(Y161L/L185H)-Heme	3.7	0.35	0.012	0.077	0.0026	0.18
Hb α (R-state) ^b	4.6 ^c		0.009 ^d		0.0016 ^e	
Mb ^{f,g}	0.51		0.019		0.030	
rMb(H64F) ^g	4.5		0.054		0.0097	

^a Number I or II indicates species I or II. ^b Human Hb α -subunit. ^c In 50 mM potassium phosphate buffer (pH 7.0, 20 °C); ref 45. ^d In 0.1 M phosphate buffer (pH 7.0, 20 °C); ref 44. ^e Calculated from $k_{\text{on}}^{\text{CO}}/k_{\text{off}}^{\text{CO}}$. ^f Sperm whale Mb. ^g In 0.1 M potassium phosphate buffer (pH 7.0, 20 °C); refs 16, 48.

rHSA(I142H/Y161L)-hemin did not show sharp resonances of the four porphyrin CH₃ groups. Other trials to convert the rHSA-(I142H/Y161L)-hemin in the low-spin azide adduct complex,³³ which is much better suited for the ¹H NMR investigation, also failed even with the addition of a large excess of ligand. In any case, the amplitude ratio of the two phases observed for the CO association to rHSA(mutant)-heme was always the same, independent of time after preparation.

O₂ and CO Binding Parameters. By analyzing the CO/O₂ competitive binding following laser flash photolysis,^{14,15} we obtained the association rate constants for O₂ ($k_{\text{on}}^{\text{O}_2}$) and the O₂ binding affinities [$P_{1/2}^{\text{O}_2} = (K^{\text{O}_2})^{-1}$] for the rHSA(I142H/Y161L)-heme, rHSA(I142H/Y161F)-heme and rHSA(Y161L/L185H)-heme (Table 2). From eq 6, variation in $k_{\text{on}}^{\text{CO}}$ arising from the two geometries of the His coordination (the faster phase is defined as species I and the slower phase is defined as species II) yielded two different O₂ binding affinities. In species I, the proximal His may coordinate to the central ferrous ion without strain, whereas in species II, the ligation may involve some distortion, resulting in weaker O₂ binding (Figure 7). The absorbance decay accompanying the CO dissociation from the rHSA(mutant)-hemeCO by the replacement with NO also showed double-exponential profiles, giving two values of $k_{\text{off}}^{\text{CO}}$ (Table 3). The proximal-side steric effect generally increases the dissociation rate for CO,^{14,15} a result that is quite consistent with our interpretation that there are two orientation isomers of the heme (the larger component of $k_{\text{off}}^{\text{CO}}$ originating from species II).

The $P_{1/2}^{\text{O}_2}$ values of the rHSA(mutant)-heme were determined to be 3–18 and 31–134 Torr for species I and II, respectively. Thus even the O₂ binding affinities of species I were 6–75-

fold lower than those of native Hb α (R-state) and Mb.^{16,40–42} Kinetically, these low affinities for O₂ were due to an 8–18-fold increase in the O₂ dissociation rate constants. Neutron diffraction studies of MbO₂ revealed that there is a direct hydrogen bond between the distal His-64 and the coordinated O₂ (Figure 7).⁴³ The high-resolution X-ray crystallographic structure of Hb α O₂ also suggested a similar interaction in the heme pocket.⁴⁴ In both hemoproteins, the distal His stabilizes the bound O₂ by about -1.4 kcal mol⁻¹ due to the hydrogen bonding. On the basis of the mutagenesis studies on sperm whale rMb, Rohlfs and co-workers demonstrated that the replacement of His-64 with apolar amino acid residues (Leu or Phe) results in loss of the hydrogen bonding, and markedly increased the O₂ dissociation rates (342–833-fold higher than Mb).¹⁶ In the rHSA(mutant)-heme, the dioxygenated heme is buried in the core of the hydrophobic cavity without any counterpart for the hydrogen bond; thus the even small $k_{\text{off}}^{\text{O}_2}$ values for species I are greater than those of Hb α and Mb. In species II, the proximal-side steric effect could further increase the dissociation rates and cause a large decline in the O₂ binding affinity. In contrast, the binding parameters of CO to the rHSA(mutant)-heme (species I) exhibited similar values of Hb α (≤ 3 -fold),^{45,46} because the coordinated CO in Hb α does not form a hydrogen bond with the distal His-64.⁴⁷

Comparison of the O₂ binding parameters for rHSA(I142H/Y161L)-heme and rHSA(I142H/Y161F)-heme shows that the presence of a Phe rather than Leu at position 161 results in 6-fold and 4-fold increases in the O₂ binding affinity for species I and II, respectively. This is mainly due to an increase in the O₂ association rate constant (Table 2). The same trend was observed for CO binding (3-fold increase in $k_{\text{on}}^{\text{CO}}$) (Table 3). The substitution of Leu-161 (102 Å³) by Phe-161 (137 Å³)⁴⁹ replaces an isopropyl group with a rigid benzyl group within the heme pocket. In I142H/Y161L, the small side-chain of Leu-161 may allow free rotation of the side-chain of neighboring Leu-185, thereby reducing the volume on the distal-side of the porphyrin plane (Figure 7). Actually, modeling and experimental studies suggest that His-185 in Y161L/L185H can coordinate to the central ferrous ion of the heme. On the other hand, the bulkier aromatic side-chain of Phe-161 may prevent rotation of the isopropyl group of Leu-185 and thereby provide greater room of the distal pocket; this might allow easier access to the heme Fe atom and account for the increased association rates for O₂ and CO.

Conclusion

HSA exploits weak axial coordination by Tyr-161 to bind hemin into the heme pocket. Reduction of the central ferric ion partly disrupts the Fe–O(phenolate) bond and produces unusual

- (40) Gibson, Q. H. *J. Biol. Chem.* **1970**, *245*, 3285–3288.
 (41) Olson, J. S.; Andersen, M. E.; Gibson, Q. H. *J. Biol. Chem.* **1971**, *246*, 5919–5923.
 (42) Imai, K.; Morimoto, H.; Kotani, M.; Watari, H.; Hirata, W.; Kuroda, M. *Biochim. Biophys. Acta* **1970**, *200*, 189–197.
 (43) Phillips, S. E. V.; Schoenborn, B. P. *Nature* **1981**, *292*, 81–82.
 (44) Shaanan, B. *J. Mol. Biol.* **1983**, *171*, 31–59.
 (45) Steinmeier, R. C.; Parkhurst, L. J. *Biochemistry* **1975**, *14*, 1564–1571.
 (46) Sharma, V. S.; Schmidt, M. R.; Ranney, H. M. *J. Biol. Chem.* **1976**, *251*, 4267–4272.
 (47) Hanson, J. C.; Schoenborn, B. P. *J. Mol. Biol.* **1981**, *153*, 117–146.
 (48) rMb(H64L) exhibited an abnormally large CO binding affinity and $k_{\text{on}}^{\text{CO}}$ compared to those of other mutants; ref 16.
 (49) Creighton, T. E. *Proteins: Structures and Molecular Properties*; W. H. Freeman and Co.: New York, 1983; p 242.

ferrous four-coordinate intermediate-spin state hemoprotein. We have engineered mutant rHSA-heme complexes which can bind O₂ reversibly with an affinity that is only 1 order of magnitude lower than the affinity of O₂ for Hb α (R-state) and Mb. The principal modifications to the heme pocket that are required to confer reversible O₂ binding are (1) replacement of Tyr-161, the endogenous anionic nucleophile, by hydrophobic amino acid (Leu or Phe), and (2) introduction of His as a proximal base at position Ile-142 or Leu-185 (either side of the porphyrin ring plane). The transport of O₂ by the rHSA-heme could be of tremendous clinical importance not only as a red cell substitute but also as an O₂-providing therapeutic reagent. Although a number of Hb-based O₂ carriers have already been developed, the administration of these materials often elicits an acute increase in blood pressure by vasoconstriction.^{50–52} This side-effect is caused by the rapid capture of the endothelial-derived relaxing factor, namely NO, by Hb that has leaked through the vascular endothelium. In contrast, our rHSA(mutant)-heme would not induce such hypertension, because the albumin carrier has low permeability through the muscle capillary pore.⁵³

(50) Tsuchida, E. Perspectives of Blood Substitutes. In *Blood Substitutes: Present and Future Perspectives*; Tsuchida, E., Ed.; Elsevier Science: Lausanne, 1998; pp 1–14.

(51) Winslow, R. M. *Annu. Rev. Med.* **1999**, *50*, 337–353.

(52) Squires, J. E. *Science* **2002**, *295*, 1002–1005.

(53) Tsuchida, E.; Komatsu, T.; Matsukawa, Y.; Nakagawa, A.; Sakai, H.; Kobayashi, K.; Suematsu, M. *J. Biomed. Mater. Res.* **2003**, *64A*, 257–261.

Our results on several mutants have also shown that modification of the distal-side of the heme pocket has a measurable effect on O₂ binding affinity (compare Leu-161 and Phe-161). To develop this promising O₂ carrier as a blood substitute, further work using a combined mutagenic and synthetic approach is required; (1) additional mutations, e.g. an introduction of a distal base which in Mb and Hb α forms a hydrogen bond with the coordinated O₂, may help to stabilize the O₂ adduct complex, and (2) small modifications to the heme structure designed to adjust its position within the pocket interior but without straining the proximal His coordination, may improve and modulate the O₂ binding ability. To aid these modifications, crystal structural analysis of rHSA(mutant)-heme complexes is now underway.

Acknowledgment. This work was supported by a Grant-in-Aid for Scientific Research (No. 16350093) from JSPS, a Grant-in-Aid for Exploratory Research (No. 16655049) from MEXT Japan, Health Science Research Grants (Regulatory Science) from MHLW Japan, and Wellcome Trust (UK). The work at Imperial College London was partially carried out as the Japan-UK Research Cooperative Program (Joint Project) of JSPS.

Supporting Information Available: UV–vis absorption and MCD spectra of FePPIXDME, MCD spectra of the ferric rHSA-(mutant)-hemin and aquo-metMb. This material is available free of charge via the Internet at <http://pubs.acs.org>.

JA054819U